Hypertension

ORIGINAL ARTICLE

Microbial Metabolite 4EPS Inhibits AT1R to Reduce Blood Pressure and Aortic Aneurysm Outcome

Terri J. Harford, Khuraijam Dhanachandra Singh, Triveni R. Pardhi, Russell Desnoyer, Tarun Ravi, Zaira Palomino Jara, Ajay Zalavadia, Kate Stenson, Sathyamangla V. Naga Prasad, Sadashiva S. Karnik

BACKGROUND: Plasma accumulation of the gut microbial metabolite 4-ethylphenylsulfate (4EPS), derived from dietary amino acid, tyrosine, has been associated with cardiovascular, renal, metabolic, and neurological disorders. AngII (angiotensin II) infusion increases circulating 4EPS in mice, suggesting a potential mechanistic role. We hypothesized that 4EPS modulates AngII-regulated pathophysiology and disease progression by directly inhibiting AT1R (angiotensin II type 1 receptor).

METHODS: This hypothesis was tested by combining AT1R pharmacology, cell signaling assays, ex vivo vascular studies, an AngII-induced aortic aneurysm growth model, and plasma proteomics analysis.

RESULTS: in vitro, 4EPS reduced the binding of both AngII and the antagonist candesartan to AT1R and suppressed AngII-induced calcium signaling. Ex vivo, 4EPS attenuated AngII-mediated vasoconstriction. In vivo, high-fat diet–fed ApoE-null mice coinfused with AngII and 4EPS showed significant blunting of blood pressure elevation and a marked reduction in aortic aneurysm–related mortality compared with mice infused with AngII alone. Analysis of aortic remodeling revealed increased elastin preservation and decreased thickening of the intimal and medial layers in 4EPS-treated animals. Plasma proteomics indicated alterations in actin–cytoskeletal signaling pathways consistent with reduced activation of ERK (extracellular-regulated kinase) 1/2, filamin-A, and proteins involved in vascular smooth muscle cell motility.

CONCLUSIONS: These findings identify 4EPS as a benign, endogenous AT1R antagonist that diminishes AngII-mediated hemodynamic and vascular pathology. By suppressing cytoskeletal signaling associated with vascular remodeling, 4EPS provides significant protection against hypertension and aortic aneurysm progression in mice, revealing a previously unrecognized protective role for a gut microbial metabolite in modulating renin-angiotensin system activity. ***(Hypertension.* 2026;83:00–00. DOI: 10.1161/HYPERTENSIONAHA.125.25364.)** • **Supplement Material**.

Key Words: amino acids ■ angiotensin II ■ aortic aneurysm ■ gastrointestinal microbiome ■ proteomics

The renin-angiotensin system (RAS) regulates ambient changes in blood pressure (BP) and cardiovascular health through hormone AngII (angiotensin II).[1] Dysregulation of AngII signaling can lead to a wide spectrum of cardiovascular diseases (CVD).[2–4] Recent studies in mice raised in germ-free and conventional environments suggested that responses to AngII, such as BP elevation, reactive oxygen species generation, vascular inflammation, immune cell infiltration into tissues, fibrosis of the heart and kidneys, and end-organ damage, are subdued in germ-free mice.[1–7] The germ-free mouse studies thus suggested that microbiota affects the balance of benefits and risks of AngII on CVD outcomes.

Metabolism of dietary protein, lipid, and polysaccharides by gut microbial flora is strongly linked to the cause of diseases, including CVD,[1,5,8] obesity,[6,7] and type 2 diabetes.[8] For instance, microbial metabolism of aromatic amino acids,[9–11] branched-chain amino acids,[12–14] short-chain fatty acids,[15–17] and N-acyl amides[18] influence BP,[1,19–21] kidney functions,[22] insulin sensitivity, and

Correspondence to: Sadashiva S. Karnik, PhD, Cardiovascular and Metabolic Sciences, Room NB50-76, Cleveland Clinic, Cleveland, OH 44095. Email karniks@ccf.org
Supplemental Material is available at https://www.ahajournals.org/doi/suppl/10.1161/HYPERTENSIONAHA.125.25364.
For Sources of Funding and Disclosures, see page XXX.

Hypertension is available at www.ahajournals.org/journal/hyp

NOVELTY AND RELEVANCE

What Is New?

We provide novel evidence that the microbial metabolite 4-ethylphenylsulfate (4EPS) directly binds to AT1R (angiotensin II type 1 receptor), disrupting angiotensin binding and suppressing vascular contractile response to AngII (angiotensin II). This is the first demonstration that coinfusion of 4EPS with AngII inhibits blood pressure elevation in male mice and significantly attenuates both the pathophysiology and mortality associated with aortic aneurysm growth in a validated mouse model.

What Is Relevant?

Humoral influences of microbial metabolites on host physiology and pathology are increasingly recognized, yet the underlying mechanisms remain poorly understood. Our findings identify 4EPS as a symbiotic modulator capable of attenuating blood pressure and aortic aneurysm progression. Unlike synthetic angiotensin receptor blockers, which broadly suppress both harmful and beneficial AT1R signaling, 4EPS may offer a more biologically harmonious approach to antagonize AT1R.

Clinical/Pathophysiological Implications?

4EPS represents a promising therapeutic candidate. The development of more potent 4EPS analogs could establish a novel class of pharmacological tools that complement existing antihypertensive therapies while preserving beneficial AT1R (angiotensin II type 1 receptor) signaling, offering a foundation for microbiota-inspired drug discovery aimed at improving cardiovascular outcomes.

Nonstandard Abbreviations and Acronyms

4EPS	4-ethylphenylsulfate
AA	aortic aneurysm
ACE	angiotensin-converting enzyme
AngII	angiotensin II
AngIV	angiotensin 3-8 (Val-Tyr-Ile-His-Pro-Phe)
ARB	angiotensin receptor blocker
ASD	autism spectrum diseases
AT1R	AngII type 1 receptor
BP	blood pressure
CKD	chronic kidney disease
Col3A1	collagen 3a1
Colα1a	collagen α1a
CVD	cardiovascular disease
ERK	extracellular-regulated kinase
FlnA	filamin A
GPCR	G-protein coupled receptors
HEK293	human embryonic kidney 293
HFD	high-fat diet
KIM-1	kidney injury marker 1
MAPK	mitogen-activated protein kinase
MOVAS	mouse aortic vascular smooth muscle
RAS	renin-angiotensin system
SMA	smooth muscle actin
TGFβ	transforming growth factor beta

glucose homeostasis[23] in mice. Gut microbiome–induced trimethylamine-*N*-oxide production promotes development of atherosclerosis in mice.[11,24–26] Human studies have examined the effects of several types of dietary components on CVDs.[11,27] However, our understanding of the mechanism of microbial-metabolite interactions with RAS in CVD is a knowledge gap that has greatly limited clinical translational studies.

GPCRs (G-protein coupled receptors) mediate both positive and negative effects on host-health for several microbial metabolites. For example, phenylacetylglutamine and phenylacetylglutamate are enriched in type 2 diabetes, linked to CVD, and modulate adrenergic receptor signaling in vivo.[2,28–30] The short-chain fatty acids,[16,31] butyrate, propionate, and acetate modulate BP and cardiovascular health, via the GPCRs,[16,32] Gpr41[33] and Olfr78.[34,35] A recent study showed a significant alteration in several microbial metabolites, including an increase of 4-ethylphenylsulfate (4EPS) in wild-type C57BL/6J mice in response to AngII infusion.[19] 4EPS is a gut microbial metabolic product of the dietary protein aromatic amino acid tyrosine (Tyr).[11] Elevated level of 4EPS is observed in CVD,[11] chronic kidney disease (CKD),[36–38] BP regulation,[39] and autism spectrum diseases (ASD).[19,40] Despite these important insights, the molecular target and mechanisms by which 4EPS influences host physiology and function are unknown.

In this study, we tested the hypothesis that 4EPS directly interacts with AT1R (angiotensin type 1 receptor). It is a GPCR component of RAS responsible for vascular response to AngII. The hormone-binding pocket of

AT1R contains distinct subpockets that engage Tyr[4] and Phe[8] of AngII—residues critical for receptor activation. Due to its structural similarity to these amino acid side-chains, 4EPS may bind to one or both subpockets and antagonize AngII-induced AT1R activation. We show that 4EPS is a benign antagonist orthosteric ligand of AT1R, reduces AT1R-binding of partial agonist, AngIV (angiotensin 3-8 [Val-Tyr-Ile-His-Pro-Phe]), and inverse agonist, candesartan. 4EPS inhibits AngII-induced mobilization of calcium in cells, contraction of vessels ex vivo, and an increase in acute systolic BP and diastolic BP in vivo. Coadministration of AngII+4EPS inhibits chronic elevation of BP and mitigates aortic aneurysm (AA) growth in a mouse model of AA, with no adverse effects on cardiac and renal functions. These findings suggest a potential protective role played by elevated circulating levels of 4EPS in reducing the health risks associated with AngII overactivity. Thus, our study provides specific insights into how 4EPS influences host physiology and pathology through benign antagonism of AT1R.

METHODS

For detailed methods, see the text and cited references in the Supplemental Material.[41–43] The authors declare that all supporting data are included within the article and the Supplemental Material.

Cell Culture

HEK293 (human embryonic kidney 293) cells stably expressing rat AT1aR protein were grown in Dulbecco's Modified Eagle Media (DMEM, Invitrogen) supplemented with 10% fetal bovine serum and G418 (1 mg/mL). Mouse vascular aortic smooth muscle cells were acquired from the ATCC (catalog no. ATCC CRL-2797).[41,42] These cells are immortalized aortic smooth muscle cells from mice, using SV40 large T antigen. Mouse aortic vascular smooth muscle (MOVAS) cells obtained from ATCC and cultured in DMEM were tested for AT1R functional state did not show a measurable Ca^{2+} response. MOVAS cells were then transfected with pcDNA-HA-AT1aR expression plasmid that contained hygromycin resistance. The MOVAS-AT1R clone stably expressing HA-AT1R, as determined by FACS analysis using the anti–HA-Alexa Fluor 488 (catalog 349 no. 2350S; Cell Signaling Technology, Danvers, MA) were grown in DMEM containing 0.2 mg/mL G418 and 200 µg/mL hygromycin. The EA.hy926 endothelial cells (ATCC CRL-2922) were cultured in DMEM supplemented with 10% fetal bovine serum. During experiments, serum was withdrawn for 3 hours (HEK: AT1aR) or 24 hours (MOVAS-AT1R) before treatment/assessment as indicated.

Statistical Analysis

All statistical analysis was performed using GraphPad Prism 10. Data are summarized as means±SEM with $P<0.05$ value set as significant. Significant values are also displayed as $^{*}P<0.05$, $^{**}P\leq0.01$, $^{***}P\leq0.001$, and $^{****}P\leq0.0001$ in relevant places in the text and figures. Normality of the distribution of data was confirmed using the D'Agostino-Pearson normality test. Student *t* test was used when comparing 2 variables. Comparison of >2 variables was performed with 1-way ANOVA with Dunnett multiple comparison test when the normality test passed. If normality was not achieved, 1-way ANOVA was performed using Kruskal Wallace followed by Dunnett multiple comparison. Concentration-response curves were done using nonlinear regression, and normality was also tested using the D'Agostino-Pearson normality test. Tail-cuff BP was analyzed by 1-way ANOVA followed by the Tukey test.

RESULTS

4EPS Reduces AngII Interaction With AT1R

Cheema and Pluznick[19] previously reported that multiple microbial metabolites are increased in the plasma metabolome of AngII-infused C57BL/6J mice. We studied 6 significantly increased metabolites shown in Figure 1 for their direct influence on AngII activation of AT1R. HEK293 cells stably expressing rat AT1aR (HEK-AT1R, ≈5 pmol/mg) were used as a model to measure changes in AngII-dependent intracellular Ca^{2+} response. The concentrations of the 6 metabolites chosen in the calcium mobilization experiments were based on clinical values reported in disease states. If the disease values are not reported, we used ≈100-fold increase over the concentration found in nondisease human plasma.[11] The effects of various metabolites on AT1R activation by AngII were monitored by EC_{50} shift (AngII potency change) and E_{max} change (AngII efficacy change). Together, these parameters characterize the overall effect of metabolites on Ca^{2+} response to AngII in the HEK-AT1R cells across a range of concentrations (Figure 1). The Ca^{2+} response was inhibited ≈10-fold by 4EPS ($P<0.0001$) and <2-fold by PCG ($P=0.0034$) when compared with the AngII+vehicle–treated cells. The E_{C50} shift was not significant in treatment with the remaining 4 metabolites. The E_{max} was decreased significantly by 4EPS ($P=0.0002$) and PCS ($P<0.0001$) when compared with the AngII+vehicle treatment. PCG and PCS are uremic toxins known to cause detrimental effects to cells in cardiorenal diseases at 5-fold lower concentrations (0.0041 mg/dL) than what we used in our assay.[35–39] However, the antagonist-like effect of 4EPS on AngII-induced Ca^{2+} response is novel, and it looked a lot like the pharmacological effects of an established antagonist, olmesartan, on EC_{50} and E_{max}. We, therefore, selected 4EPS for further investigation in this study by first confirming that AngII and 4EPS did not elicit a Ca^{2+} response in HEK cells not expressing the rat AT1aR. Second, we confirmed that the inhibitory effect of 4EPS was not due to a cytotoxic effect (Figure S1).

To test the hypothesis that 4EPS interferes with AngII binding to antagonize AT1R function, we performed ligand binding studies using the partial agonist

ORIGINAL ARTICLE

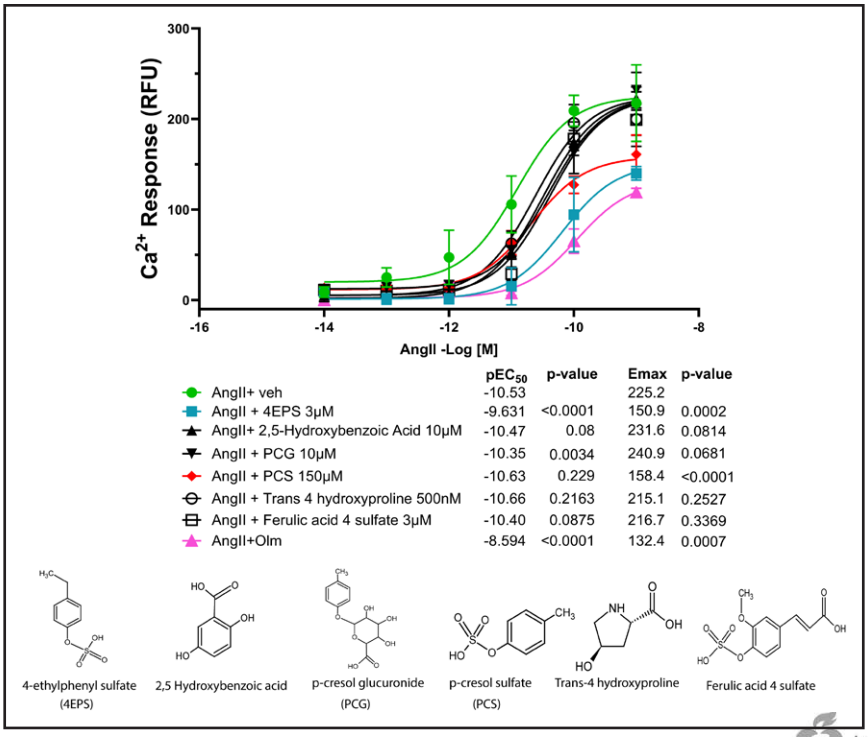

Figure 1. Effect of microbial metabolites on AngII (angiotensin II)-mediated AT1R (angiotensin II type 1 receptor) activation monitored by Ca^{++} release assay.

Top, The HEK293 (human embryonic kidney 293)–AT1R cells were preincubated with vehicle (normal saline), olmesartan (OLM; 100 nM), or metabolites, incubated with calcium 5 dye, and then stimulated with indicated doses of AngII in triplicate, in 3 independent experiments (n=3), as described previously.[41,44,45] The concentration of 4-ethylphenylsulfate (4EPS) and other metabolites used was selected based on reported clinical values in disease states, representing approximately a 100-fold increase over concentrations observed in nondisease human plasma.[11] Each metabolite+AngII dose, along with respective vehicle-only controls, was tested in separate triplicate wells (noncumulative dose-response protocol) to prevent the influence of receptor desensitization and AT1R tachyphylaxis. Intracellular calcium changes were quantified as $\Delta F/F$ (F_{max}–F_{min}) and reported as calcium response (RFU [relative fluorescence units]) using FlexStation3 equipped with SoftMax Pro software, as authenticated in previous studies.[44,45] The concentration-response data analysis was performed using GraphPad Prism 10 nonlinear regression comparison. **Middle**, The EC_{50} shift and E_{max} change for calcium response to AngII on compound treatment were assessed to determine *P* values shown in the table (n=3). Using the clonally selected HEK-AT1R line minimizes biological heterogeneity and provides reproducible higher signaling amplitude in this assay. However, future work using primary cells or multiple cell lines would extend the generalizability of 4EPS effect on AT1R signaling to assess biological variabilities, including genetic variation and the influence of sex. **Bottom**, Structures of bacterially derived metabolites shown.

^{125}I-AngIV. The lower affinity of ^{125}I-AngIV compared with ^{125}I-AngII makes it a preferred probe for evaluating a benign antagonist (4EPS) in the binding experiment. Total membrane isolated from MOVAS stably expressing AT1aR was used for saturation binding assays. MOVAS-AT1R cells are a model of vascular smooth muscle that form the basis for vascular tone and BP. Reduction of ^{125}I-AngIV binding in the presence of 4EPS (1 mM) was significant (*P<0.05, ****P<0.001) as seen in Figure 2A. Next, competition binding assays were performed. The antagonist tracer ^{3}[H]-Candesartan displacement by Sar1-AngII±4EPS showed an increase in the inhibitory concentration (IC_{50}) values in the presence of 4EPS and 4EPS analogs (Figure 2B). However, the change in IC_{50} did not reach significance (P=0.07). The reasons may be technical, that is, [Sar1]AngII binding is stronger than candesartan. Also, the higher receptor density in the membranes may mask the benign inhibitory effect of 4EPS.

Molecular modeling and unbiased docking analyses indicated that 4EPS occupies a subpocket within the orthosteric ligand binding site of AT1R (Figure 3; Figure S2). This subpocket accommodates the Phe^{8}-COO^{-} sidechain of AngII and AngIV, as well as the biphenyl imidazole scaffold of angiotensin receptor blockers (ARBs), such as candesartan and olmesartan (Figure S2). Occupancy of this subpocket by 4EPS is facilitated by AT1R residues Arg^{167}, Lys^{199}, and Trp^{84} (Figure S2). Previous studies have shown that mutagenesis of Arg^{167}, Lys^{199}, and Trp^{84} produce nonfunctional AT1R protein,[42] precluding the mutagenesis approach to validate 4EPS-AT1R docking model. We developed an innovative pharmacological approach[43,46–50] described below to circumvent this hurdle.

Using SciFinder, we searched for 4EPS-like molecules in chemical space, identified 54 compounds, and performed induced-fit docking to AT1R (Figure S2). This analysis indicated that the docking score of 5

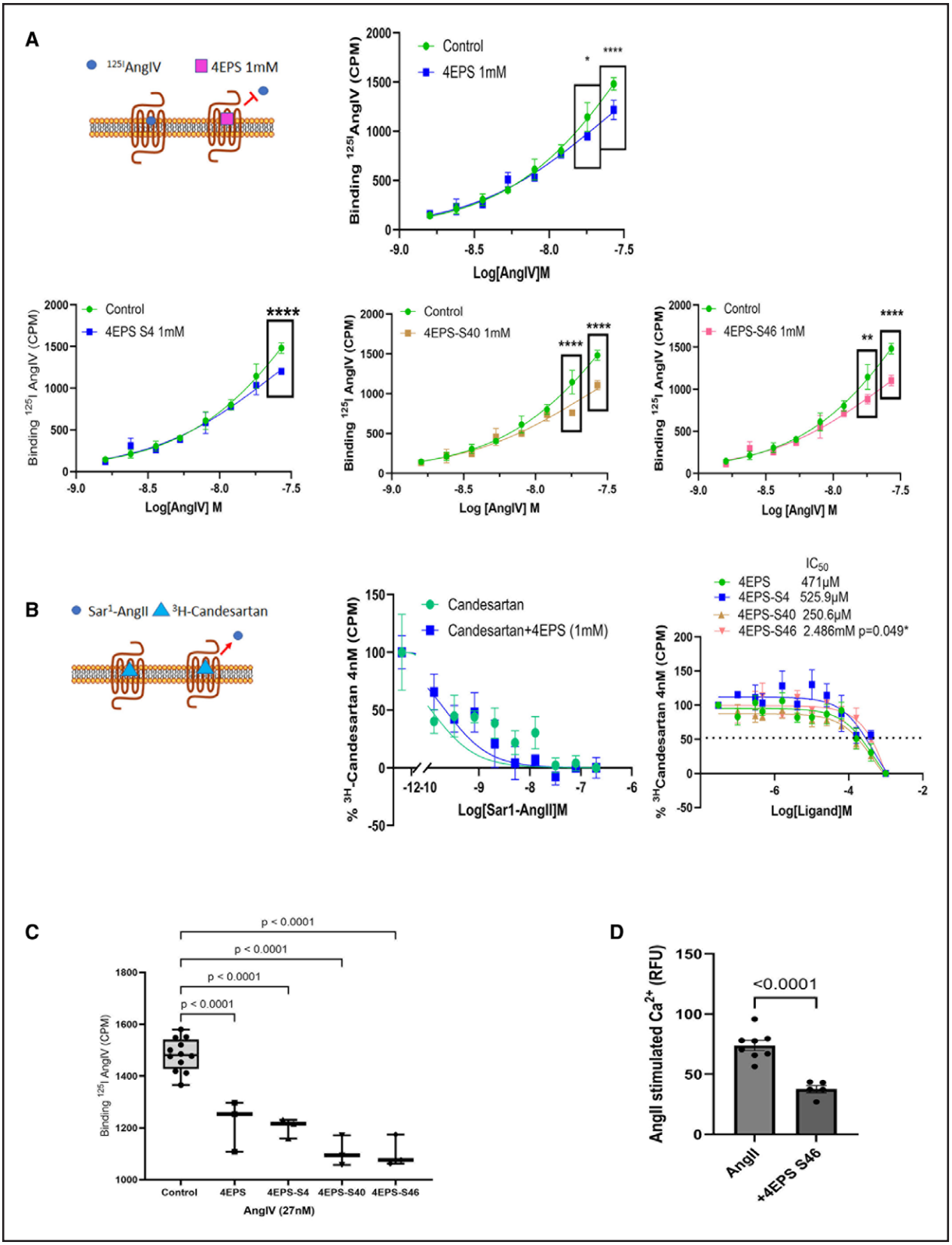

Figure 2. Effect of 4-ethylphenylsulfate (4EPS) and analogs on orthosteric ligand binding to AT1R (angiotensin II type 1 receptor): these studies were performed using mouse aortic vascular smooth muscle (MOVAS)–AT1R cells, which are a model of vascular smooth muscle that form the basis for vascular tone and blood pressure as described previously.[41,45]

A, The saturation binding assays used MOVAS-AT1R membranes incubated with orthosteric partial agonist, ^{125}I-AngIV (control) concentrations ranging between 1.6 and 27 nM (specific activity, 16 Ci/mmol) in the presence of 1 mM of 4EPS and the 4EPS analogs, (*Continued*)

compounds (Table S1) was higher than 4EPS. Of these, only S4, S40, and S46 were commercially available as potential tools to pharmacologically interrogate the 4EPS binding site of AT1R. In ^{125}I-AngIV binding analysis, S4, S40, and S46 (1 mM) reduced the binding of radioligand (Figure 2A). Order of inhibitory potency was S46 ≈ S40 > S4≈4EPS, which indicated that replacement of the ethyl group in 4EPS by tertbutyl in S4 had a minor effect, and replacement with bulkier phenyl in S46 and benzyl in S40 had a larger effect (Figure 2C). In the ^{3}H-Candesartan tracer displacement, in the presence of 4EPS, S4, S40, and S46, inhibitory potency of S46 >S4≈4EPS>S40 was observed (Figure 2B, right), again showing S46 having the greatest effect in displacement. As compound S46 was most effective at displacement, we evaluated S46 effects on AT1R activation using the calcium assay and found that this compound inhibited the response in HEK-AT1aR cells (Figure 2D). Due to the limited availability of pharmaceutical-grade S46, we did not perform detailed ex vivo and animal studies on the S46 compound. The studies below focus on the natural microbial metabolic product, 4EPS.

4EPS Reduces AngII-Induced Vascular Reactivity Ex Vivo

The initial ex vivo wire myography analysis of the iliac artery and abdominal aorta from naïve mice is shown in Figure S3. As described previously,[41] integrity of endothelium and the vessel-wall was assessed by measuring contraction/relaxation responses to treatment of high potassium physiological salt solution followed by phenylephrine and acetyl- β-methyl choline. To ensure that the changes in vasoconstriction were AT1R specific, contraction of aortic explants was then assessed using 5-HT. The contractile response for 5-HT is mediated by a distinct GPCR that signals via the Gq-protein, similar to AT1R. Dose-response curves showed that preincubation of aortic explants with 4EPS (100 µM) did not alter 5-HT–mediated vasoconstriction as compared with vehicle (Figure S4). Both vessels were then treated with multiple concentrations of 4EPS alone, which did not show vasoconstriction or relaxation response. Treatment with 300 nM AngII produced robust vasoconstriction. We observed 75% reduction (P=0.0001) at 300 µM 4EPS, and 50% reduction (P=0.001) at 150 µM in the iliac artery. When these doses were applied to the abdominal aorta, both doses resulted in ≈70% reduction (P=0.01). However, 300 µM 4EPS did not alter responses induced by 1 µM phenylephrine, 1 µM 5-HT, and 1 µM acetyl-β-methyl choline. These data indicated that the 4EPS specifically prevented AngII-induced vasoconstriction. We selected 100 µM dose of 4EPS on the abdominal aorta to conduct further studies.

Next, we evaluated the antagonism potential of 4EPS in a physiological system, mouse aortic explants from ApoE-null mice fed high-fat diet (HFD) and infused with different ligands as schematized in Figure 4A. The ApoE-null mice fed HFD represent a pathophysiological model prone to develop aortic aneurysms and vascular remodeling, along with hypertension when subjected to AngII infusion as described earlier.[41] Contractile responses were measured on 300 nM AngII stimulation in aorta explants, confirmed for integrity of the endothelium and vessel-wall by treatment with high potassium physiological salt solution followed by phenylephrine and methyl choline. A stronger contraction in response to AngII stimulation (P=0.0016) was observed in the aorta from male mice infused with AngII (1.4 mg/kg per day) for 28 days. In contrast, mice coinfused with AngII+4EPS and AngII+olmesartan elicit reduced contraction (Figure 4B, left). Interestingly, mice infused with 4EPS (2.5 mg/kg per day) alone for 28 days did not affect vascular response. When female mice were assessed, all changes to AngII (300 nM) regardless of infusion, were not significant (Figure 4B, right).

We then determined the effect of acute 4EPS (100 µM) addition in the myography chamber on contraction. Preincubation with 4EPS (100 µM) resulted in a significant reduction in AngII-mediated constriction regardless of the infusion (P=0.0001, in Figure 4C). Application of 4EPS (100 µM) alone directly to aortic segments did not affect vaso-response. Graphical representation of

Figure 2 Continued. S4, S40, and S46. **B**, The **left** cartoon shows schematic competition binding. **Middle** graph shows effect of 4EPS (1 mM) on competitive displacement of orthosteric antagonist, [^{3}H]-candesartan (4 nM) by 0.04 to 1000 nM concentrations of [Sar1] AngII (angiotensin II) under equilibrium conditions. Two independent experiments were performed, each with triplicate, and the resulting specific binding values were pooled to generate the displayed curves. Binding kinetics analyzed by the nonlinear curve-fitting program GraphPad Prism 10 suggested that 4EPS competed [^{3}H]-candesartan binding. **Right** graph shows the effect of 1 nM to 1 mM 4EPS analogs on direct binding of [^{3}H]-candesartan (4 nM). The binding kinetics were analyzed by the nonlinear curve-fitting program and Student t test to determine mean IC_{50} values indicated for each analog using the GraphPad Prism 10 program. **C**, Analysis of significance of inhibition of ^{125}I-AngIV binding caused by 4EPS and 4EPS analogs. One-way ANOVA with Dunnett test was used to determine significance of the decrease of ^{125}I-AngIV binding in boxed data points in **A**, which compares ^{125}I-AngIV only and AngIV+4EPS or analogs. **D**, Significant inhibition of orthosteric full-agonist ligand, AngII-induced AT1R activation by the most potent metabolite analog, 4EPS-S46. More detailed ex vivo and animal studies on S46 will be possible only when enough pharmaceutical-grade compound is commercially available. Current studies focus on the naturally produced microbial metabolic product, 4EPS. The ^{125}I-AngIV binding assay used 1 mmol/L 4EPS to test potential antagonistic effects at the highest achievable concentration under controlled in vitro conditions for maximal interrogation for proof-of-concept. In contrast, live cell functional assays apply a dynamic 4EPS range to avoid nonpharmacological effects associated with high concentrations. RFU indicates relative fluorescence unit.

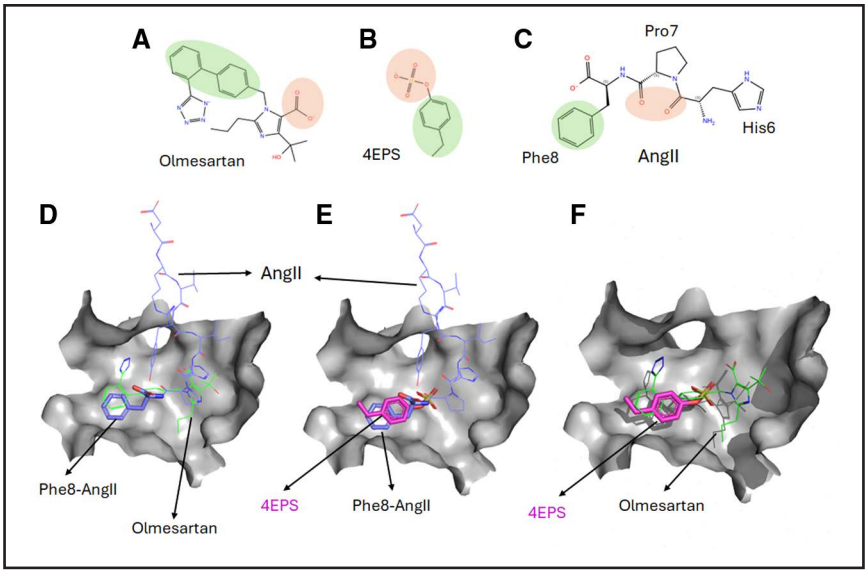

Figure 3. Model of 4-ethylphenylsulfate (4EPS) interaction with the orthosteric pocket of AT1R (angiotensin II type 1 receptor). Chemical structure of olmesartan (OLM; **A**), 4EPS (**B**), and the last 3 residues of AngII (angiotensin II; **C**). Modeled docking poses[42,43,46–55] of indicated ligands within the orthosteric ligand binding pocket of AT1R (**D** through **F**). The green regions represent hydrophobic areas, whereas the orange regions indicate hydrophilic areas. The ethylphenyl group of 4EPS occupies the position of Phe^8 in AngII and the biphenyl position in OLM. The sulfate group of 4EPS takes the place of the backbone carbonyls of Pro7-His6 in AngII and the carboxylic group of OLM, indicating that 4EPS has inhibitory potential against both AngII and angiotensin receptor blockers. The gray surface in **D** through **F** represents the protein interface with orthosteric ligands, AngII, 4EPS, and ARBs.

contraction curves depicted in Figure 4D shows that preincubation with 4EPS resulted in a reduction in vasoconstriction induced by AngII. Both male and female ApoE-null mice fed a HFD were used in the myography experiments. Female data shows poor response to AngII; for instance, the effect of AngII stimulation was not significant (P=0.4140) in female mice aorta explants.

4EPS Reduces AngII-Induced Increase of BP

Telemetry monitored acute BP response in mice indicated that IP injection of either AngII alone or AngII+4EPS causes a transient increase in BP. In mice coinfused with AngII+4EPS, a significant reduction in the change of systolic BP (P=0.0199), diastolic BP (P=0.0106), and MAP (P=0.0176) was observed when compared with mice infused with AngII alone (Figure 5A). However, the inhibition of acute BP increase by 4EPS is significantly weaker compared with AngII+olmesatran coinfusion.

Chronic BP changes in mice were measured by the noninvasive tail-cuff method using the chronic infusion protocol schematized in Figure 4A. Basal BP readings were taken 10 days into HFD, and elevated BP readings were taken at 14 and 28 days after osmotic pump implantation. Body weight and the weight of organs in the mice on HFD, infused for 28 days with vehicle, AngII, 4EPS, AngII+4EPS, and AngII+olmesartan, were not significantly affected (Figure S5). Systolic BP significantly increased at 14 (P=0.0246) and 28 days (P=0.0013) of AngII infusion, diastolic pressure increased at 28 days (P=0.0308), and mean pressure increased significantly at 14 (P=0.0220) and at 28 days (P=0.0002) of AngII infusion when compared with basal BP. In mice coinfused with AngII+4EPS, there was no significant increase in all 3 BP parameters (Figure 5). Together, these observations suggest that coinfusion with 4EPS blocked the hemodynamic effects of AngII, which is similar to the effect of ARB, olmesartan.

4EPS Reduces AngII-Induced Aortic Aneurysm Formation in ApoE-Null Mice

We determined the effects of 4EPS on AngII-induced AA in ApoE-null male mice maintained on HFD. Five 28-day treatment groups described in the methods received either vehicle, AngII, AngII+4EPS, 4EPS alone, or AngII+olmesartan. 100% of mice survived in the vehicle (n=12), 4EPS alone (n=7), and AngII+olmesartan (n=6) groups. In the AngII group (n=16), 50% mortality was recorded. The mortality in the AngII+4EPS group (n=14) was 14.3%, suggesting substantial (P=0.0488) protection by 4EPS (Figure 6A). Coinfusion with 4EPS did not cause any change in the weights of liver, spleen, lungs, heart, and kidneys, normalized to overall body weights. However, overall body weight was reduced in AngII, AngII+4EPS, and 4EPS only groups, which may be due to lean/fat mass changes (Figure S5). In the female ApoE-null mice infused with AngII, coinfused with 4EPS or olmesartan, no significant change was observed.

AA growth progression in mice was monitored by measuring the maximal aortic lumen diameter using ultrasonography with the Vevo2100 echocardiography

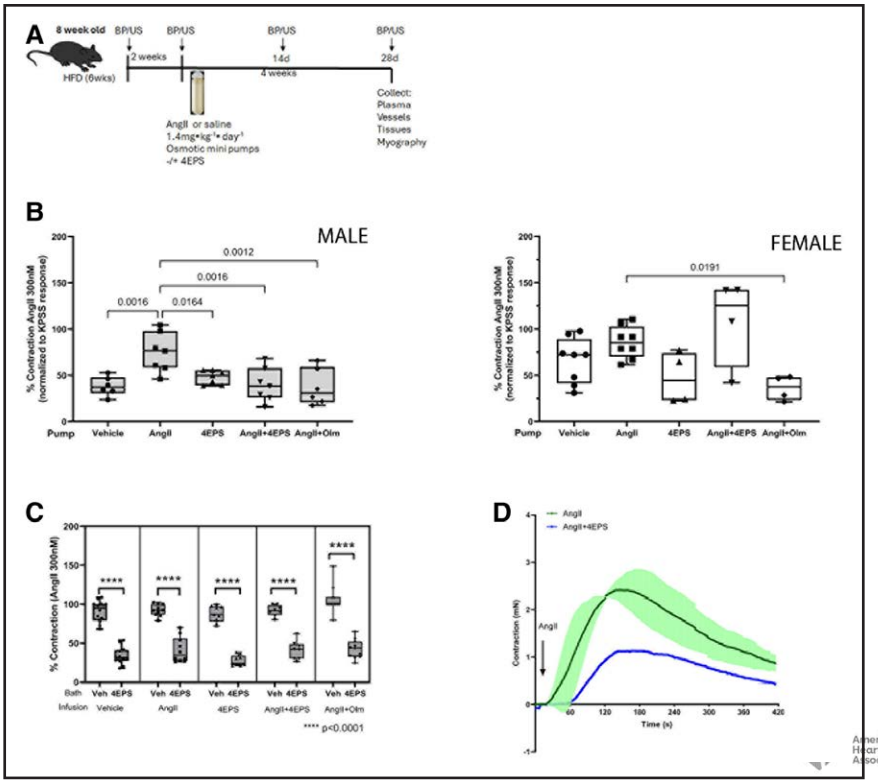

Figure 4. Ex vivo assessment of 4-ethylphenylsulfate (4EPS) effect on aortic contractile response to AngII (angiotensin II). **A**, Graphical experimental design. ApoE-null mice on high-fat diet (HFD) were infused with AngII (1.4 mg/kg per day) vehicle or 4EPS (2.5 mg/kg per day) for 4 weeks. **B**, Wire myography measured vascular contraction of infrarenal abdominal aorta (2 sections, 2 mm apart were used per mouse) in male mice, shaded (n=5–7), female mice, unshaded (n=3–8), infused with ligands as indicated, and stimulated with AngII (300 nM). Average value of 2 sections from each mouse was used in aortic contractile response calculations. Magnitude of contraction (mN, milli-Newton; max-min) was normalized to maximal contraction caused by high potassium physiological salt solution (KPSS). Significance was calculated using 1-way ANOVA with Dunnett test compared with vehicle-infused using GraphPad Prism. **C**, Vasoconstriction was assessed in male mice pretreated with vehicle or 4EPS (100 µM) before stimulation with AngII (n=7–8). Graph depicts percent contraction, with 300 nM AngII-induced contraction in vehicle-pretreated mice as 100%. **D**, Graphical representation of AngII contraction response observed in a representative mouse aortic ring recorded with LabChart. After initial quality assessment (see methods), each vessel was first exposed to 300 nM AngII, then washed and allowed to recover (assessed by KPSS response) before AngII (300 nM)+4EPS (100 µM) cotreatment (blue curve). After another wash and recovery, a final 300 nM AngII response was recorded. Green graph shows mean±variation of initial and final AngII responses. Vehicle vs 4EPS effects were analyzed using Student *t* test. BP indicates blood pressure; and OLM, olmesartan.

system (Visualsonics). AngII infusion led to increased suprarenal abdominal aortic diameter at both 14 (1.5-fold increase, P=0.0133) and 28 days (2-fold increase, P<0.0005). In contrast, a significant increase (1.3X increase, P=0.0147) in lumen diameter was observed at only 28 days, which suggests delays in the progression of abdominal aortic aneurysms in the AngII+4EPS group (Figure 6B). Histopathology analysis employing Aperio ImageScope circumvents problems for accurate measurements of intima/media in the hematoxylin and eosin–stained sections. Examination of suprarenal abdominal aortic sections demonstrated a significant (P=0.0099) thickening of the aortic wall intima/media layers associated with thrombus in AngII-infused mice (Figure 6C). Evidence of elastolysis was assessed by monitoring changes in elastin content and structural alterations within the tunica, media layers of the aorta, by Aperio ImageScope. Elastin content measurement showed a significant decrease in the AngII-infused group compared with AngII+4EPS, 4EPS, AngII+olmesartan, and the vehicle control group (P<0.0001). Infusion with 4EPS, AngII+4EPS, and AngII+olmesartan did not significantly differ as compared with the vehicle control group (P=0.9711, P=0.9996, P=0.8832, respectively; Figure 6D). Again, infusion of 4EPS alone exhibited no alterations to intima/media thickness, elastin area, and elastin scoring, supporting it being a benign antagonist.

4EPS Alters Molecular Pathways Underlying AngII-Induced AA

Unbiased proteomic analysis on the mice plasma of AngII+4EPS compared with AngII treatment groups identified potential molecular signaling mechanisms[51–55,61–74] responsible for reduced vascular remodeling. Significantly altered protein data (Table S2) was analyzed by Ingenuity Pathway Analysis, String, and GO

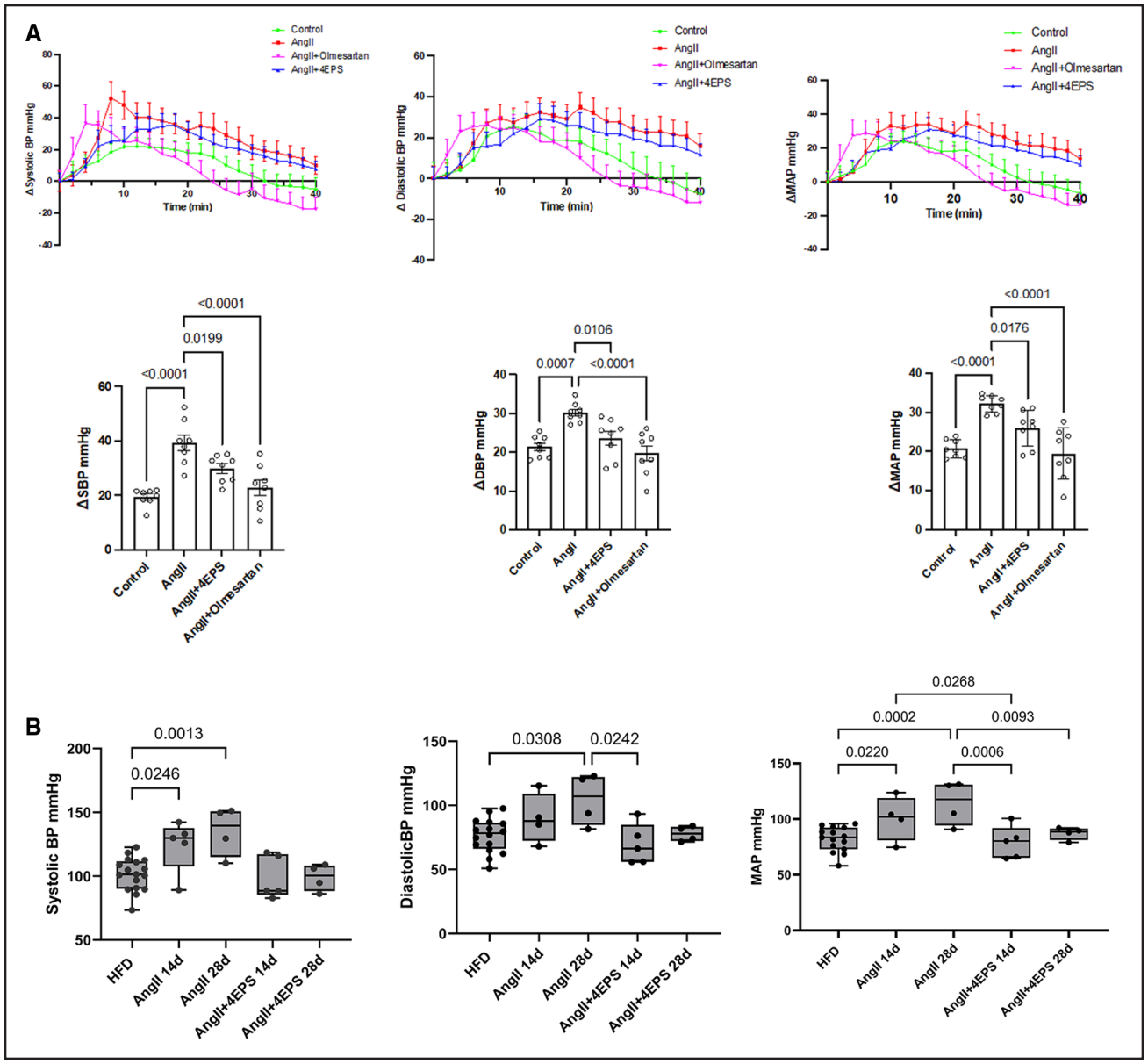

Figure 5. Acute and chronic blood pressure (BP) response to 4-ethylphenylsulfate (4EPS) coinfusion with AngII (angiotensin II). Treatment with 4EPS alone did not cause BP change in mice under acute and chronic experimental setups, but 4EPS coinfusion with AngII interfered with BP change. To account for variability in acute BP response due to first-pass metabolism of compounds in the liver and proteolytic processing of AngII in the endothelium by ACE2 (angiotensin-converting enzyme 2), the mice in each treatment group were given the same treatments on 3 separate days. **A**, Systolic BP (SBP) and diastolic BP (DBP) monitored by radiotelemetry in conscious freely moving mice in response to acute treatment. C57B6 mice were given 50 µL bolus IP injections of saline, AngII (0.2 mg/kg), AngII+4EPS (0.2 and 0.4 mg/kg respectively), and AngII+olmesartan (OLM; 0.2 mg/kg and 0.4 mg/kg, respectively) while pressure was monitored. Three mice per group, each given the same treatments on 3 separate days, allowing 48 hours in between treatments. Telemetry data collection and analysis are described in the methods. Telemetry raw data is shown in Figure S10. The ΔSBP, ΔDBP, and ΔMAP traces show Average±SE of a total of 9 readings/treatment group. The bar graphs show changes in SBP and DBP from baseline, and the significance of difference is calculated using an average of 8 consecutive points at peak response. Analysis performed by 1-way ANOVA with Dunnett posttest using GraphPad Prism. **B**, BP changes measured by the CODA noninvasive tail-cuff method in response to 14- and 28-day chronic infusions in ApoE-null male mice. Mice on high-fat diet (HFD) were infused with vehicle (saline), 4EPS 2.5 mg/kg per day, AngII (1.4 mg/kg per day), AngII+4EPS (AngII 1.4 mg/kg per day, 4EPS 2.5 mg/kg per day). Please note that HFD and HFD+4EPS treatments in mice did not show any change in BP in 28 days. Analysis performed by 1-way ANOVA with Tukey posttest using GraphPad Prism.

to identify altered canonical pathways, diseases and biological functional responses to our treatments. The key canonical pathways identified were in actin cytoskeleton signaling and ERK (extracellular-regulated kinase)/MAPK (mitogen-activated protein kinase) signaling. Alteration in biofunction pathways involves changes in chemotaxis of blood cells (granulocytes, neutrophils, phagocytes), adhesion property of vascular endothelial cells, production of

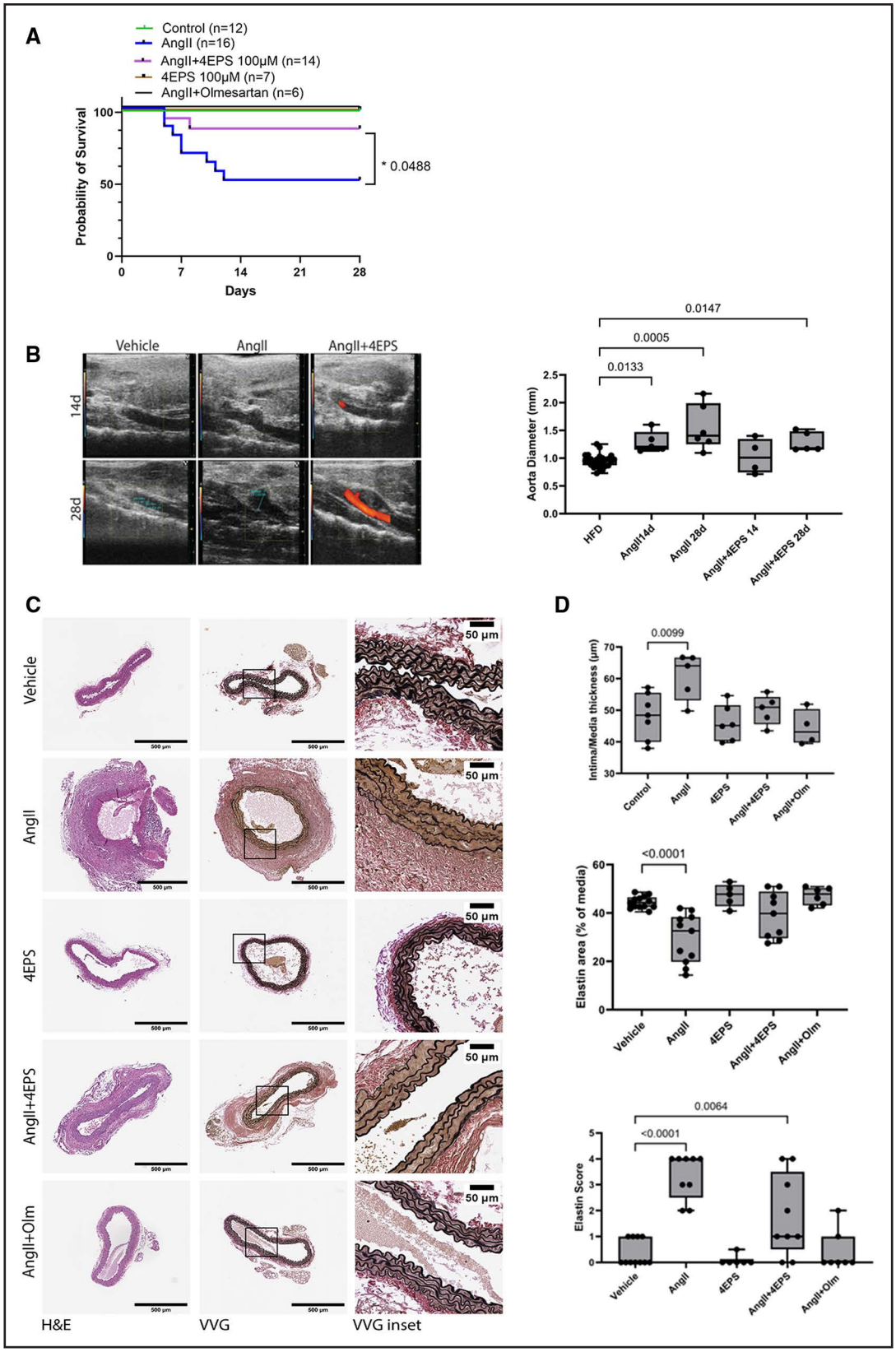

Figure 6. Effect of 4-ethylphenylsulfate (4EPS) on survival and pathology of AngII (angiotensin II) induced aneurysm. ApoE-null mice on high-fat diet (HFD) for 2 weeks were implanted with osmotic pumps for infusion of indicated ligands for 28 days. **A**, Kaplan-Meier simple survival curves were generated in GraphPad Prism 10 using Log-rank test for significance, n=6–16 based on treatment groups. Survival in 4EPS cotreatment group was same as that of the saline and AngII+olmesartan (OLM) groups. **B**, Representative long-axis ultrasound images of aortic lumen diameter monitored on days 14 and 28, as described previously.[56] (*Continued*)

NO, and reactive oxygen species. In the String database analysis, the top hit identified was molecules associated with elastin fibers and kidney disease. GO analysis elucidated changes associated with integrin signaling, blood coagulation, and inflammation (Figure S6). Gene Ontology analysis of 4EPS treatment led to alterations in only 8 unique products in total, as compared with AngII+4EPS with 57 products (Figure S6A).

The predicted 4EPS influence on AngII-induced actin-cytoskeletal signaling may be relevant to understanding vascular wall remodeling changes observed in the 4EPS+AngII coinfused mice in Figure 6. Using the MOVAS-AT1R cells, we monitored cell migration capability (see methods) in a wound-healing assay shown in Figure S7. MOVAS-AT1R cells, growth arrested in serum-free media, were incubated with saline control, AngII (1 µm), or AngII+4EPS (100 µm) over 24 hours. Images were acquired at 0, 8, and 24 hours. Cell migration is observed in all treatment conditions. However, AngII+4EPS treatment diminished migration of cells when compared with the AngII alone treatment, which substantially increased migration capability in comparison to saline control. As expected, treatment with 4EPS (100 µm) alone showed no changes in migration capability as compared with AngII.

Next, we monitored alterations in expression and phosphorylation of FlnA (filamin A), a key actin cross-linking biomechanical signal transducer protein, which has been associated with changes in hypertension and CVDs.[51,52] AngII activation increases FlnA phosphorylation and recruitment to AT1R, which is known to be crucial for regulating the actin cytoskeleton dynamics. Treatment of MOVAS-AT1R cells with AngII increased phosphorylation of FlnA in comparison to treatment with AngII+4EPS (Figure S8A). There was no significant effect on FlnA expression. These data suggest that 4EPS directly inhibits AT1R-FlnA-cytoskeleton coupling induced by AngII. As the proteomic analysis suggested alterations in ERK/MAPK signaling, ERK expression and phosphorylation were assessed (Figure S8B and S8C). ERK phosphorylation is critical for the increase in Ca^{2+}_i stimulated smooth muscle contractions. In both MOVAS AT1R and HEK-AT1R cells, AngII treatment led to an increase in ERK phosphorylation as compared with AngII+4EPS.

Our plasma proteomics data indicated an inverse association of 4EPS with chronic renal impairment, in contrast to literature reports that indicated a positive correlation with CKD and end-stage renal disease. We assessed circulating 4EPS levels in our experimental mice by measuring plasma 4EPS by mass spectrometry (Figure S9A). We observed that AngII-treated mice exhibited ≈2 ng/mL of 4EPS. This is a ≈7-fold (P=0.0148) increase of 4EPS in plasma compared with vehicle-treated mice, similar to that reported in a study by Cheema and Pluznick.[19] Plasma 4EPS levels significantly exceeded in AngII+4EPS coinfused mice (200 ng/mL; P<0.0001) than 4EPS only infused mice (≈30 ng/mL; P=0.0003). This striking increase suggests that 4EPS clearance may be impaired in this treatment group. Consistent with this speculation, a study by Emans et al[74] reported reduced glomerular filtration rate in rats after 8 days of AngII infusion via osmotic minipumps.[75] Similarly, Xu et al[75] demonstrated alterations in kidney function markers in C57BL/6 mice treated with AngII at the same dose used in our study.[76] Together, these findings support the hypothesis that elevated plasma 4EPS levels in the AngII+4EPS group may result from reduced renal clearance due to AngII-induced kidney dysfunction.

To evaluate potential renal dysfunction, we assessed markers of kidney damage by monitoring mRNA levels of Colα1a (collagen α1a), TGFβ (transforming growth factor beta), KIM-1 (kidney injury marker 1), and SMA (smooth muscle actin; Figure S9B). There was no change in Colα1a or TGFβ in AngII, AngII+4EPS, and AngII+olmesartan treatment. However, AngII infusion led to a significant increase in KIM-1 and SMA, with no concurrent change in AngII+4EPS infusion. These observations suggest potential retention of 4EPS in circulation in the AngII+4EPS coinfused mice but lack of 4EPS-associated renal injury.

DISCUSSION

Our lead-off question was whether the microbial metabolites reported by Cheema and Pluznick[19] directly

Figure 6 Continued. The lumen diameters outlined in red were measured using Vevo Lab software on images acquired on Vevo2100 using ms550 probe. Aortic lumen diameter changes in different treatment groups (n=4–6) compared with HFD are indicated; significance was determined using 1-way ANOVA and Tukey multiple comparison test using GraphPad Prism 10. **C**, Representative images of hematoxylin and eosin (H&E)–stained and Verhoeff-vanGieson staining (VVG)–stained infrarenal segment of Aorta tissue from different treatment groups, with scale bar 300 µm as described in earlier studies.[41,57–60] **D**, Serial sections of aorta images were used for analysis of intima/media thickness. For assessment of wall thickness, media/intima measurements were taken from 4 to 6 serial images/animal (n=4–6 mice per group). Average thickness of aorta in a mouse is calculated from 40 measurement bars placed per image. Elastin measurement was performed blinded by our histology core, using image analysis software scoring for the entire area of VVG stain per image, as described in earlier articles.[56–58] A total of 6 to 13 images/group was used to calculate the elastin area/animal (4–6 mice per group). Please note that ImageScope, powered by a machine learning algorithm, was employed to circumvent problems for accurate measurements of intima/media in the H&E-stained sections and elastin content in VVG-stained sections. In addition, visual elastin scoring of deidentified images was also performed by 4 independent reviewers by inspecting 7 to 11 images per treatment group. Data analysis was performed using 1-way ANOVA with Dunnett multiple comparison test using GraphPad Prism 10.

modulate AT1R signaling underlying the vaso-regulatory actions of AngII. Using the HEK-AT1R cell signaling platform—where AngII stimulation elicits a transient and saturable calcium response—we demonstrated that only 4EPS out of the 6 microbial metabolites tested (Figure 1) significantly reduced both the EC_{50} and E_{max} for AT1R activation by AngII. The calcium responses to AngII and AngII+4EPS were dependent on AT1R expression in HEK cells, and inhibition by the ARB, olmesartan was more potent than that produced by 4EPS. Although interference with AT1R signaling by 4EPS suggests functional interaction, whether 4EPS directly binds to AT1R is not established by signaling studies. Radioligand-binding studies in MOVAS-AT1R cell membrane provided evidence for 4EPS direct binding to AT1R. Specific binding of the partial agonist ^{125}I-AngIV was systematically reduced by 4EPS (Figure 2A). Displacement of the AT1R blocker ^{3}H-candesartan by [Sar^{1}]AngII was accelerated (left-shifted) in the presence of 4EPS in competitive binding assays (Figure 2B), suggesting that 4EPS interferes with the binding of both ARBs and AngII. Previous mutagenesis and structural studies have defined discrete orthosteric binding sites for ARBs and AngII.[42,51,52] Unbiased in silico docking analysis confirmed that 4EPS interacts with AT1R residues Arg167, Lys199, and Trp84—key components of the orthosteric binding pocket (Figure 3; Figure S2B). These residues also engage 4EPS like all established orthosteric ligands. In the model, 4EPS occupies the same space that accommodates the Phe8 residue of AngII critical for receptor activation,[53] which explains the molecular basis of competitive inhibition exerted by 4EPS. The predicted molecular interaction was further validated by a series of 4EPS analogs (Figure S2A). Analogs bearing bulkier benzyl and phenyl substitutions exhibited stronger inhibition of ^{125}I-AngIV binding than analogs with smaller ethyl or tertbutyl groups (Figure 2A), consistent with stronger predicted binding in silico. Furthermore, the 4EPS-S46 inhibited AT1R activation more potently (Figure 2D).

Collectively, these results demonstrate that 4EPS directly binds within the orthosteric pocket of AT1R, by sterically hindering the interaction of ARBs as well as AngII-Phe8 with AT1R, thereby attenuating activation of AT1R signaling by AngII. 4EPS may also interfere with AT1R inhibition by ARBs. Thus, 4EPS acts as a benign antagonist of AngII signaling. The discovery that a gut-derived microbial metabolite can function as a benign AT1R antagonist represents a novel mechanism of host-microbe interaction targeting the RAS. The physiological implications of this effect are discussed below.

We next assessed the physiological relevance of this mechanism by measuring ex vivo vascular response and in vivo BP response (Figures 4 and 5). Ex vivo wire myography revealed that 4EPS significantly (P=0.0016) reduced contraction of aortic rings from AngII-infused mice. Acute treatment with 4EPS diminished AngII-induced contractile responses by ≈50% (P<0.0001; Figure 4B). In vivo, 4EPS coinfusion with AngII markedly blunted increases in systolic, diastolic, and mean arterial pressures (Figure 5). Importantly, 4EPS alone had no effect on basal vascular tone or BP, indicating that 4EPS inhibitory action is AngII-dependent. These results are consistent with the cellular findings and suggest that 4EPS exerts a humoral effect that modulates host vascular responses via inhibition of AT1R signaling.

To further explore the in vivo pathophysiological relevance, we examined the effect of 4EPS on AngII-induced abdominal AA formation in HFD-fed ApoE-null genotype mice, an experimental AA model that recapitulates human risk factors such as hypercholesterolemia, obesity, and hypertension.[61–63] Coinfusion of 4EPS prevented AngII-induced elevations in systolic, diastolic, and mean arterial pressures (Figure 5B) compared with the elevated BP response on AngII-infused control mice. Mass spectrometry confirmed significant increases in plasma 4EPS levels in AngII, 4EPS, and AngII+4EPS groups (Figure S9A), supporting the conclusion that attenuation of AngII-induced hypertension is associated with elevated circulating 4EPS. Thus, a 4EPS increase in the plasma prevents elevation of BP. Histological analyses showed that 4EPS coinfusion prevented AngII-induced thickening of the aortic intima–media (P=0.0099) and loss of elastin content (P=0.001; Figure 6), both indicators of vascular remodeling and a precursor to the progression of AA.[63–66] Reduced elastin content reflects elastolysis and weakening of aortic wall which has been associated with increased aneurysm dissection, hypertension and congenital disorders including Marfan Syndrome.[64–66] Ultrasound imaging further revealed attenuation of aortic dilation in the AngII+4EPS group compared with AngII alone in 14- and 28-day groups, without changes in relative body and organ weights (Figure S5). We have previously shown that AngII infusion induces AA located in the suprarenal abdominal aortic region in 64% male ApoE-null mice on high-fat western diet.[41] In this study, the protective effect of 4EPS translated into delays in AA formation, significantly improved overall survival, with aneurysm-related mortality reduced from 50% (AngII) to 14.3% (AngII+4EPS; P=0.0488).

Proteomic analysis of plasma (Table S2) revealed that 4EPS attenuated AngII-induced activation of actin cytoskeletal signaling, consistent with preservation of vascular wall architecture. Although changes in angiotensin-converting enzyme levels were observed, their contribution to 4EPS-mediated effects requires further investigation. Functional assays demonstrated that 4EPS suppressed AngII-induced cell migration (Figure S6) and reduced phosphorylation of FlnA (Figure S7), a cytoskeletal protein known to interact with the filamin binding motif of AT1R located on its helix-8.[51,52] AT1R activation produces engagement with FlnA and induces filamin phosphorylation in cells. By dampening AT1R activation,

4EPS may inhibit downstream biomechanical signaling to the actin cytoskeleton, thereby preventing aortic wall remodeling. Recent genetic and molecular studies have shown a direct role of FlnA in AA pathology in humans and mice.[52]

Our results establish AT1R as a molecular target of 4EPS, providing mechanistic insight into the interface between gut microbial metabolites, RAS regulation, and cardiovascular functions.[1–13] It is one of a dozen possible metabolites produced by the participation of gut microbial and host enzymatic pathways. For instance, 4EPS is generated through microbial conversion of dietary tyrosine to 4-hydroxy phenylpropionic acid, and after absorption, the sulfonation reaction is performed by the host liver enzymes. Although several gut-derived metabolites have been associated with CVD risk, their direct molecular targets remain largely undefined. In this context, our identification of AT1R as a target for 4EPS provides a foundation for assessing both the potential benefits and risks of microbially derived metabolites in CVD pathophysiology.

Link between 4EPS and several neurological and psychiatric disorders, including anxiety, depression, and neurodegenerative diseases[40,67–70] may involve blood-brain barrier crossing of 4EPS. Interaction with brain AT1Rs may influence neural function and brain activity, for example, related to Autism spectrum disorders.[40,67–70] 4EPS may be a component of the gut-brain axis implicated in the regulation of stress responses and the modulation of the immune system.[71] Elevated 4EPS has been reported in CKD and heart failure[38].

Cheema and Pluznick[19] observed >8-fold increases in 4EPS in conventional mice plasma on AngII treatment. In the present study, the basal 4EPS levels in naïve C57/B6 mice were below the level of detection, and AngII infusion increased the plasma 4EPS levels ≈2- to 8-fold (P=0.0148), whereas AngII+4EPS coinfusion resulted in an ≈80-fold elevation (P=<0.0001; Figure S9). Notably, 4EPS coinfusion attenuated markers of kidney injury, indicating possible reno-protective effects that merit future investigation.

If 4EPS acts as a benign antagonist of AT1R, whether 4EPS is elevated in disease states such as type 2 diabetes,[8] chronic heart failure,[11] neurological changes,[40] and CKD[38] represents a pathogenic factor, or an adaptive compensatory response remains unclear. Human metabolome databases reported that plasma 4EPS concentrations in healthy humans range from 0.02 to 0.03 μM, and its levels linked to diseases are not established.[11] Our experimental infusions achieved a 40- to 80-fold elevation, which was AA protective (Figure S8A), compared with 3000% increase observed in animal models of CKD[36–39] and 40-fold increase in autism spectrum disorder (ASD) mice. Thus, 4EPS link to ASD pathogenesis was not supported in mice, and 4EPS levels were not significantly altered in patients with ASD.[67–73] Another study that linked 4EPS to reduced oligodendrocyte maturation in neurological disease referenced a 6-fold increase in plasma 4EPS in ASD children.[72,73] Importantly, large-scale clinical studies found no association between 4EPS levels and major adverse cardiovascular events, including myocardial infarction, stroke, and mortality.[8,11] These findings, together with our data, suggest that elevated 4EPS exerts protective or adaptive effects against AngII-mediated vascular injury. Outside of a therapeutic window, whether a high plasma concentration of 4EPS is pathogenic needs further studies.

Receptor specificity analyses indicate that 4EPS does not inhibit vasoconstriction induced by phenylephrine or serotonin, arguing against significant interaction with amine GPCRs. Computational modeling predicted low affinity for AT2R and no interaction with MAS or MAS-related GPCRs. Given that AT2R blockade exacerbates aneurysm formation,[41] the protective actions of 4EPS are likely mediated through AT1R rather than AT2R. Ongoing studies aim to determine whether 4EPS modulates other GPCR targets.

In summary, our in vitro, ex vivo, and in vivo data together support the conclusion that AT1R is the molecular target of 4EPS. Both the calcium messenger signaling and the biomechanical signal transduction through protein-protein interaction triggered by AT1R are attenuated by 4EPS. Elevation of 4EPS in some disease states may provide an adaptive advantage.

Limitations

This study shows the benign antagonism mechanism of 4EPS on AngII-mediated AT1R signaling through in vitro and cell-based experiments. However, translating these findings to physiological and pathological settings in vivo reveals a sex-dependent effect. In male mice, 4EPS effectively mitigates AngII-induced aortic contraction, BP elevation, and AA progression, consistent with its role as a benign antagonist. In contrast, a muted 4EPS effect in female mice may seem confounding. Previous studies have shown that females exhibit a diminished AngII/AT1R response due to several factors, including the influence of sex hormones on gene expression and increased gene dosage of the AT2R, which is encoded on the X chromosome.[76–79] AT2R is a well-known physiological antagonist of AT1R. Taken together, the protective effects of 4EPS are pronounced in males and likely masked in females. Further studies will be necessary to clarify the observed divergence in vascular response to AngII and 4EPS between males and females.

Perspectives

Hypertension is a major contributor to diseases, and growing evidence links gut microbiome-derived metabolites to the pathology of CVDs. Among these, the 4EPS

level has been observed to increase in CVD, CKD, ASD, and hypertension, leading to the prevailing assumption that 4EPS effects are deleterious. However, the role of 4EPS, particularly in relation to the RAS and its molecular targets, remained unclear. We investigated whether 4EPS interacts with AT1R and studied its impact on AngII-induced signaling, vasoconstriction, and AA formation in mice. The results indicate that, contrary to prevailing assumptions 4EPS is mechanistically protective rather than harmful. Notably, while elevated 4EPS has been linked to disease states, its causal role remains unproven in human studies, and associations with conditions such as T2DM, congestive heart failure, and CKD are not firmly established. Thus, 4EPS may function as an endogenous antagonist of AngII under normal conditions, with its regulation potentially disrupted during disease. Furthermore, the discovery that 4EPS interferes with the binding of ARBs raises important clinical implications, indicating that plasma levels of 4EPS could influence the efficacy of ARB-based therapies. If 4EPS is excessively reduced or scavenged outside of a defined therapeutic window, disease outcomes could worsen. Our study challenges conventional interpretations of 4EPS as a harmful metabolite and proposes that harnessing the gut microbiome's capacity to produce beneficial molecules like 4EPS may offer a novel therapeutic approach for treating CVD.

ARTICLE INFORMATION

Received May 22, 2025; accepted January 5, 2026.

Affiliation

Cardiovascular and Metabolic Sciences Department, Lerner Research Institute, Cleveland Clinic, OH.

Acknowledgments

The authors express their appreciation to the Proteomics core for their assistance in LC-MS analysis and the Imaging Core for their assistance with analysis of histological images; Renliang Zhang for assistance with LC-MS quantitation of 4-ethylphenylsulfate, and Ling Li for assistance with the quantitative proteomics; Lousie Lantier and the Vanderbilt University Mouse Metabolic Phenotyping Center (RRID: SCR_021939) for assistance with the telemetry blood pressure study; and LRI core facilities including the Animal Core Facility, the Histopathology and Biomedical Engineering Imaging Core. The authors are especially indebted to Maya Camhi for immunohistochemistry assistance and Judith Drazba for assistance in imaging and image analysis studies.

Sources of Funding

This work was supported by National Institutes of Health (NIH) RO1 grants, HL142091 and HL132351 to S.S. Karnik. Proteomics core supported by NIH grant S10 OD030398 BBW to Belinda Willard. Ultrasonography was supported by Vevo instrumentation grant 1S10OD021561 (SVP) to S.V. Naga Prasad. The Vanderbilt Mouse Metabolic Phenotyping Center is supported by NIH grants, DK135073, DK020593.

Disclosures

None.

Supplemental Material

Supplemental Methods
Tables S1–S2
Figures S1–S10
References 11,40,41,43–50,56–60,70,72,73

REFERENCES

1. Kent Z, Aknnola OM, Ahlidja W, Bina J. Food as medicine for hypertension: microbiota as mediators. *Hypertension*. 2025;82:1569–1589. doi: 10.1161/HYPERTENSIONAHA.125.17950
2. Witkowski M, Weeks TL, Hazen SL. Gut microbiota and cardiovascular disease. *Circ Res*. 2020;127:553–570. doi: 10.1161/circresaha.120.316242
3. Zhu W, Gregory JC, Org E, Buffa JA, Gupta N, Wang Z, Li L, Fu X, Wu Y, Mehrabian M, et al. Gut microbial metabolite TMAO enhances platelet hyperreactivity and thrombosis risk. *Cell*. 2016;165:111–124. doi: 10.1016/j.cell.2016.02.011
4. Jiang S, Shui YJ, Cui Y, Tang C, Wang XH, Qiu XY, Hu WP, Fei LY, Li Y, Zhang SP, et al. Gut microbiota dependent trimethylamine N-oxide aggravates angiotensin II-induced hypertension. *Redox Biol*. 2021;46:102115. doi: 10.1016/j.redox.2021.102115
5. Yang T, Santisteban MM, Rodriguez V, Li E, Ahmari N, Carvajal JM, Zadeh M, Gong M, Qi Y, Zubcevic J, et al. Gut dysbiosis is linked to hypertension. *Hypertension*. 2015;65:1331–1340. doi: 10.1161/HYPERTENSIONAHA.115.05315
6. Durgan DJ, Ganesh BP, Cope JL, Ajami NJ, Phillips SC, Petrosino JF, Hollister EB, Bryan RM Jr. Role of the gut microbiome in obstructive sleep apnea-induced hypertension. *Hypertension*. 2016;67:469–474. doi: 10.1161/HYPERTENSIONAHA.115.06672
7. Backhed F, Ding H, Wang T, Hooper LV, Koh GY, Nagy A, Semenkovich CF, Gordon JI. The gut microbiota as an environmental factor that regulates fat storage. *Proc Natl Acad Sci U S A*. 2004;101:15718–15723. doi: 10.1073/pnas.0407076101
8. Larsen N, Vogensen FK, van den Berg FWJ, Nielsen DS, Andreasen AS, Pedersen BK, Abu Al-Soud W, Sorensen SJ, Hansen LH, Jakobsen M. Gut microbiota in human adults with type 2 diabetes differs from non-diabetic adults. *PLoS One*. 2010;5:e9085. doi: 10.1371/journal.pone.0009085
9. Liu Y, Hou Y, Wang G, Zheng X, Hao H. Gut microbial metabolites of aromatic amino acids as signals in host-microbe interplay. *Trends Endocrinol Metab*. 2020;31:818–834. doi: 10.1016/j.tem.2020.02.012
10. Dodd D, Spitzer MH, Van Treuren W, Merrill BD, Hryckowian AJ, Higginbottom SK, Le A, Cowan TM, Nolan GP, Fischbach MA, et al. A gut bacterial pathway metabolizes aromatic amino acids into nine circulating metabolites. *Nature*. 2017;551:648–652. doi: 10.1038/nature24661
11. Nemet I, Li XMS, Haghikia A, Li L, Wilcox J, Romano KA, Buffa JA, Witkowski M, Demuth I, König M, et al. Atlas of gut microbe-derived products from aromatic amino acids and risk of cardiovascular morbidity and mortality. *Eur Heart J*. 2023;44:3085. doi: 10.1093/eurheartj/ehad333
12. Huang Y, Zhou M, Sun H, Wang Y. Branched-chain amino acid metabolism in heart disease: an epiphenomenon or a real culprit? *Cardiovasc Res*. 2011;90:220–223. doi: 10.1093/cvr/cvr070
13. Uddin GM, Zhang L, Shah S, Fukushima A, Wagg CS, Gopal K, Al Batran R, Pherwani S, Ho KL, Boisvenue J, et al. Impaired branched chain amino acid oxidation contributes to cardiac insulin resistance in heart failure. *Cardiovasc Diabetol*. 2019;18:86. doi: 10.1186/s12933-019-0892-3
14. Walejko JM, Christopher BA, Crown SB, Zhang GF, Pickar-Oliver A, Yoneshiro T, Foster MW, Page S, van Vliet S, Ilkayeva O, et al. Branched-chain alpha-ketoacids are preferentially reaminated and activate protein synthesis in the heart. *Nat Commun*. 2021;12:1680. doi: 10.1038/s41467-021-21962-2
15. Whelton SP, Hyre AD, Pedersen B, Yi Y, Whelton PK, He J. Effect of dietary fiber intake on blood pressure: a meta-analysis of randomized, controlled clinical trials. *J Hypertens*. 2005;23:475–481. doi: 10.1097/01.hjh.0000160199.51158.cf
16. Natarajan N, Hori D, Flavahan S, Steppan J, Flavahan NA, Berkowitz DE, Pluznick JL. Microbial short chain fatty acid metabolites lower blood pressure via endothelial G protein-coupled receptor 41. *Physiol Genomics*. 2016;48:826–834. doi: 10.1152/physiolgenomics.00089.2016
17. Shubitowski TB, Poll BG, Natarajan N, Pluznick JL. Short-chain fatty acid delivery: assessing exogenous administration of the microbiome metabolite acetate in mice. *Physiol Rep*. 2019;7:e14005. doi: 10.14814/phy2.14005
18. Cohen LJ, Esterhazy D, Kim SH, Lemetre C, Aguilar RR, Gordon EA, Pickard AJ, Cross JR, Emiliano AB, Han SM, et al. Commensal bacteria make GPCR ligands that mimic human signalling molecules. *Nature*. 2017;549:48–53. doi: 10.1038/nature23874
19. Cheema MU, Pluznick JL. Gut microbiota plays a central role to modulate the plasma and fecal metabolomes in response to angiotensin II. *Hypertension*. 2019;74:184–193. doi: 10.1161/HYPERTENSIONAHA.119.13155
20. Joe B, McCarthy CG, Edwards JM, Cheng X, Chakraborty S, Yang T, Golonka RM, Mell B, Yeo JY, Bearss NR, et al. Microbiota introduced to germ-free rats restores vascular contractility and blood pressure. *Hypertension*. 2020;76:1847–1855. doi: 10.1161/HYPERTENSIONAHA.120.15939

21. Lin H, Chen J, Ma S, An R, Li X, Tan H. The association between gut microbiome and pregnancy-induced hypertension: a nested case-control study. *Nutrients*. 2022;14:4582. doi: 10.3390/nu14214582
22. GBD Chronic Kidney Disease Collaboration. Global, regional, and national burden of chronic kidney disease, 1990-2017: a systematic analysis for the Global Burden of Disease Study 2017. *Lancet*. 2020;395:709–733. doi: 10.1016/S0140-6736(20)30045-3
23. Sharma S, Tripathi P. Gut microbiome and type 2 diabetes: where we are and where to go? *J Nutr Biochem*. 2019;63:101–108. doi: 10.1016/j.jnutbio.2018.10.003
24. Koeth RA, Levison BS, Culley MK, Buffa JA, Wang Z, Gregory JC, Org E, Wu Y, Li L, Smith JD, et al. γ-Butyrobetaine is a proatherogenic intermediate in gut microbial metabolism of L-carnitine to TMAO. *Cell Metab*. 2014;20:799–812. doi: 10.1016/j.cmet.2014.10.006
25. Tang WH, Wang Z, Fan Y, Levison B, Hazen JE, Donahue LM, Wu Y, Hazen SL. Prognostic value of elevated levels of intestinal microbe-generated metabolite trimethylamine-N-oxide in patients with heart failure: refining the gut hypothesis. *J Am Coll Cardiol*. 2014;64:1908–1914. doi: 10.1016/j.jacc.2014.02.617
26. Tang WH, Wang Z, Levison BS, Koeth RA, Britt EB, Fu X, Wu Y, Hazen SL. Intestinal microbial metabolism of phosphatidylcholine and cardiovascular risk. *N Engl J Med*. 2013;368:1575–1584. doi: 10.1056/NEJMoa1109400
27. Wang Y, Chun OK, Song WO. Plasma and dietary antioxidant status as cardiovascular disease risk factors: a review of human studies. *Nutrients*. 2013;5:2969–3004. doi: 10.3390/nu5082969
28. Romano KA, Nemet I, Saha PP, Haghikia A, Li XMS, Mohan ML, Lovano B, Castel L, Witkowski M, Buffa JA, et al. Gut microbiota-generated phenylacetylglutamine and heart failure. *Circ Heart Fail*. 2023;16:e009972. doi: 10.1161/CIRCHEARTFAILURE.122.009972
29. Saha PP, Gogonea V, Sweet W, Mohan ML, Singh KD, Anderson JT, Mallela D, Witherow C, Kar N, Stenson K, et al. Gut microbe-generated phenylacetylglutamine is an endogenous allosteric modulator of β2-adrenergic receptors. *Nat Commun*. 2024;15:6696. doi: 10.1038/s41467-024-50855-3
30. Song Y, Wei H, Zhou Z, Wang H, Hang W, Wu J, Wang DW. Gut microbiota-dependent phenylacetylglutamine in cardiovascular disease: current knowledge and new insights. *Front Med*. 2024;18:31–45. doi: 10.1007/s11684-024-1055-9
31. Sanna S, van Zuydam NR, Mahajan A, Kurilshikov A, Vich Vila A, Vosa U, Mujagic Z, Masclee AAM, Jonkers D, Oosting M, et al. Causal relationships among the gut microbiome, short-chain fatty acids and metabolic diseases. *Nat Genet*. 2019;51:600–605. doi: 10.1038/s41588-019-0350-x
32. Strassheim D, Sullivan T, Irwin DC, Gerasimovskaya E, Lahm T, Klemm DJ, Dempsey EC, Stenmark KR, Karoor V. Metabolite G-Protein coupled receptors in cardio-metabolic diseases. *Cells Basel*. 2021;10: doi: 10.3390/cells10123347
33. Dinakis E, Nakai M, Gill PA, Yiallourou S, Sata Y, Muir J, Carrington M, Head GA, Kaye DM, Marques FZ. The gut microbiota and their metabolites in human arterial stiffness. *Heart Lung Circ*. 2021;30:1716–1725. doi: 10.1016/j.hlc.2021.07.022
34. Shepard BD, Koepsell H, Pluznick JL. Renal olfactory receptor 1393 contributes to the progression of type 2 diabetes in a diet-induced obesity model. *Am J Physiol Renal Physiol*. 2019;316:F372–F381. doi: 10.1152/ajprenal.00069.2018
35. Liabeuf S, Glorieux G, Lenglet A, Diouf M, Schepers E, Desjardins L, Choukroun G, Vanholder R, Massy ZA; European Uremic Toxin (EUTox) Work Group. Does p-cresylglucuronide have the same impact on mortality as other protein-bound uremic toxins? *PLoS One*. 2013;8:e67168. doi: 10.1371/journal.pone.0067168
36. Nemet I, Funabashi M, Li XS, Dwidar M, Sangwan N, Skye SM, Romano KA, Cajka T, Needham BD, Mazmanian SK, et al. Microbe-derived uremic solutes enhance thrombosis potential in the host. *mBio*. 2023;14:e0133123. doi: 10.1128/mbio.01331-23
37. Devlin AS, Marcobal A, Dodd D, Nayfach S, Plummer N, Meyer T, Pollard KS, Sonnenburg JL, Fischbach MA. Modulation of a circulating uremic solute via rational genetic manipulation of the gut microbiota. *Cell Host Microbe*. 2016;20:709–715. doi: 10.1016/j.chom.2016.10.021
38. Itoh Y, Ezawa A, Kikuchi K, Tsuruta Y, Niwa T. Protein-bound uremic toxins in hemodialysis patients measured by liquid chromatography/tandem mass spectrometry and their effects on endothelial ROS production. *Anal Bioanal Chem*. 2012;403:1841–1850. doi: 10.1007/s00216-012-5929-3
39. Gong J, Noel S, Pluznick JL, Hamad ARA, Rabb H. Gut microbiota-kidney cross-talk in acute kidney injury. *Semin Nephrol*. 2019;39:107–116. doi: 10.1016/j.semnephrol.2018.10.009
40. Hsiao EY, McBride SW, Hsien S, Sharon G, Hyde ER, McCue T, Codelli JA, Chow J, Reisman SE, Petrosino JF, et al. Microbiota modulate behavioral and physiological abnormalities associated with neurodevelopmental disorders. *Cell*. 2013;155:1451–1463. doi: 10.1016/j.cell.2013.11.024
41. Jara ZP, Harford TJ, Singh KD, Desnoyer R, Kumar A, Srinivasan D, Karnik SS. Distinct mechanisms of beta-arrestin-biased agonist and blocker of AT1R in preventing aortic aneurysm and associated mortality. *Hypertension*. 2023;80:385–402. doi: 10.1161/HYPERTENSIONAHA.122.19232
42. Zhang H, Unal H, Gati C, Han GW, Liu W, Zatsepin NA, James D, Wang D, Nelson G, Weierstall U, et al. Structure of the angiotensin receptor revealed by serial femtosecond crystallography. *Cell*. 2015;161:833–844. doi: 10.1016/j.cell.2015.04.011
43. Bankhead P, Loughrey MB, Fernandez JA, Dombrowski Y, McArt DG, Dunne PD, McQuaid S, Gray RT, Murray LJ, Coleman HG, et al. QuPath: open source software for digital pathology image analysis. *Sci Rep*. 2017;7:16878. doi: 10.1038/s41598-017-17204-5
44. Arkin MR, Connor PR, Emkey R, et al. FLIP assays for GPCR and ion channel targets. In: Markossian S, Grossman A, Baskir H, et al, ed. *Assay Guidance Manual*. Eli Lilly & Company and the National Center for Advancing Translational Sciences; 2004.
45. Singh KD, Jara ZP, Harford TJ, Saha PP, Pardhi TP, Desnoyer R, Karnik SS. Novel allosteric ligands of the angiotensin receptor AT1R as autoantibody blockers. *Proc Natl Acad Sci USA*. 2021;118:e2019126118. doi: 10.1073/pnas.2019126118
46. Lu C, Wu CJ, Ghoreishi D, Chen W, Wang LL, Damm W, Ross GA, Dahlgren MK, Russell E, Von Bargen CD, et al. OPLS4: Improving force field accuracy on challenging regimes of chemical space. *J Chem Theory Comput*. 2021;17:4291–4300. doi: 10.1021/acs.jctc.1c00302
47. Jacobson MP, Pincus DL, Rapp CS, Day TJF, Honig B, Shaw DE, Friesner RA. A hierarchical approach to all-atom protein loop prediction. *Proteins*. 2004;55:351–367. doi: 10.1002/prot.10613
48. Friesner RA, Banks JL, Murphy RB, Halgren TA, Klicic JJ, Mainz DT, Repasky MP, Knoll EH, Shelley M, Perry JK, et al. Glide: A new approach for rapid, accurate docking and scoring. 1. Method and assessment of docking accuracy. *J Med Chem*. 2004;47:1739–1749. doi: 10.1021/jm0306430
49. Friesner RA, Murphy RB, Repasky MP, Frye LL, Greenwood JR, Halgren TA, Sanschagrin PC, Mainz DT. Extra precision glide: docking and scoring incorporating a model of hydrophobic enclosure for protein-ligand complexes. *J Med Chem*. 2006;49:6177–6196. doi: 10.1021/jm051256o
50. Halgren TA, Murphy RB, Friesner RA, Beard HS, Frye LL, Pollard WT, Banks JL. Glide: A new approach for rapid, accurate docking and scoring. 2. Enrichment factors in database screening. *J Med Chem*. 2004;47:1750–1759. doi: 10.1021/jm030644s
51. Tirupula KC, Ithychanda SS, Mohan ML, Naga Prasad SV, Qin J, Karnik SS. G protein-coupled receptors directly bind filamin A with high affinity and promote filamin phosphorylation. *Biochemistry*. 2015;54:6673–6683. doi: 10.1021/acs.biochem.5b00975
52. Chen Y, Wei X, Zhang ZH, He Y, Huo B, Guo X, Feng X, Fang ZM, Jiang DS, Zhu XH. Downregulation of filamin A expression in the aorta is correlated with aortic dissection. *Front Cardiovasc Med*. 2021;8:690846. doi: 10.3389/fcvm.2021.690846
53. Zhang H, Unal H, Desnoyer R, Han GW, Patel N, Katritch V, Karnik SS, Cherezov V, Stevens RC. Structural basis for ligand recognition and functional selectivity at angiotensin receptor. *J Biol Chem*. 2015;290:29127–29139. doi: 10.1074/jbc.M115.689000
54. Singh KD, Unal H, Desnoyer R, Karnik SS. Mechanism of hormone peptide activation of a GPCR: angiotensin II activated state of AT_1R initiated by van der Waals attraction. *J Chem Inf Model*. 2019;59:373–385. doi: 10.1021/acs.jcim.8b00583
55. Wingler LM, Skiba MA, McMahon C, Staus DP, Kleinhenz ALW, Suomivuori CM, Latorraca NR, Dror RO, Lefkowitz RJ, Kruse AC. Angiotensin and biased analogs induce structurally distinct active conformations within a GPCR. *Science*. 2020;367:888–892. doi: 10.1126/science.aay9813
56. Wang M, Ching-Johnson JA, Yin H, O'Neil C, Li AX, Chu MWA, Bartha R, Pickering JG. Mapping microarchitectural degeneration in the dilated ascending aorta with ex vivo diffusion tensor imaging. *Eur Heart J Open*. 2023;4:oead128. doi: 10.1093/ehjopen/oead128
57. Laffey M, Tornifoglio B, Lally C. Development and initial characterization of a localized elastin degradation ex vivo porcine aortic aneurysm model. *Appl Sci*. 2023;13:9894. doi: 10.3390/app13179894
58. Stone AJ, Tornifoglio B, Digeronimo F, Shmueli K, Lally C. Quantitative susceptibility mapping of the human carotid artery: assessing sensitivity to elastin and collagen ex vivo. *Magn Reson Med*. 2025;94:771–784. doi: 10.1002/mrm.30500

59. Velenosi TJ, Hennop A, Feere DA, Tieu A, Kucey AS, Kyriacou P, McCuaig LE, Nevison SE, Kerr MA, Urquhart BL. Untargeted plasma and tissue metabolomics in rats with chronic kidney disease given AST-120. *Sci Rep*. 2016;6:22526. doi: 10.1038/srep22526
60. Yi L, Li F, Yong Y, Jianting D, Liting Z, Xuansheng H, Fei L, Jiewen L. Upregulation of sestrin-2 expression protects against endothelial toxicity of angiotensin II. *Cell Biol Toxicol*. 2014;30:147–156. doi: 10.1007/s10565-014-9276-3
61. Daugherty A, Manning MW, Cassis LA. Angiotensin II promotes atherosclerotic lesions and aneurysms in apolipoprotein E-deficient mice. *J Clin Invest*. 2000;105:1605–1612. doi: 10.1172/JCI7818
62. Rateri DL, Howatt DA, Moorleghen JJ, Charnigo R, Cassis LA, Daugherty A. Prolonged infusion of angiotensin II in apoE$^{-/-}$ mice promotes macrophage recruitment with continued expansion of abdominal aortic aneurysm. *Am J Pathol*. 2011;179:1542–1548. doi: 10.1016/j.ajpath.2011.05.049
63. Trachet B, Fraga-Silva RA, Jacquet PA, Stergiopulos N, Segers P. Incidence, severity, mortality, and confounding factors for dissecting AAA detection in angiotensin II-infused mice: a meta-analysis. *Cardiovasc Res*. 2015;108:159–170. doi: 10.1093/cvr/cvv215
64. White JV, Haas K, Phillips S, Comerota AJ. Adventitial Elastolysis Is a Primary Event in Aneurysm Formation. *J Vasc Surg*. 1993;17:371–380, discussion 380. doi: 10.1067/mva.1993.43023
65. Martyn CN, Greenwald SE. Impaired synthesis of elastin in walls of aorta and large conduit arteries during early development as an initiating event in pathogenesis of systemic hypertension. *Lancet*. 1997;350:953–955. doi: 10.1016/s0140-6736(96)10508-0
66. Iskandar Z, Dodd M, Huang J, Chin CWL, Stuart G, Caputo M, Clayton T, Child A, Jin XY, Aragon-Martin JA, et al. Exaggerated elastin turnover in young individuals with Marfan syndrome: new insights from the AIMS trial. *Eur Heart J Open*. 2023;3:oead095. doi: 10.1093/ehjopen/oead095
67. Lim S, Lee S. Chemical modulators for targeting autism spectrum disorders: from bench to clinic. *Molecules*. 2022;27:5088. doi: 10.3390/molecules27165088
68. Day F, O'Sullivan J, Pook C. 4-Ethylphenol-fluxes, metabolism and excretion of a gut microbiome derived neuromodulator implicated in autism. *Front Mol Biosci*. 2023;10:1267754. doi: 10.3389/fmolb.2023.1267754
69. Timperio AM, Gevi F, Cucinotta F, Ricciardello A, Turriziani L, Scattoni ML, Persico AM. Urinary untargeted metabolic profile differentiates children with autism from their unaffected siblings. *Metabolites*. 2022;12:797. doi: 10.3390/metabo12090797
70. Needham BD, Funabashi M, Adame MD, Wang Z, Boktor JC, Haney J, Wu WL, Rabut C, Ladinsky MS, Hwang SJ, et al. A gut-derived metabolite alters brain activity and anxiety behaviour in mice. *Nature*. 2022;602:647–653. doi: 10.1038/s41586-022-04396-8
71. Ntranos A, Park HJ, Wentling M, Tolstikov V, Amatruda M, Inbar B, Kim-Schulze S, Frazier C, Button J, Kiebish MA, et al. Bacterial neurotoxic metabolites in multiple sclerosis cerebrospinal fluid and plasma. *Brain*. 2022;145:569–583. doi: 10.1093/brain/awab320
72. Kang DW, Adams JB, Vargason T, Santiago M, Hahn J, Krajmalnik-Brown R. Distinct fecal and plasma metabolites in children with autism spectrum disorders and their modulation after microbiota transfer therapy. *mSphere*. 2020;5:e00314–e00320. doi: 10.1128/mSphere.00314-20
73. Needham BD, Adame MD, Serena G, Rose DR, Preston GM, Conrad MC, Stewart Campbell A, Donabedian DH, Fasano A, et al. Plasma and fecal metabolite profiles in autism spectrum disorder. *Biol Psychiatry*. 2021;89:451–462. doi: 10.1016/j.biopsych.2020.09.025
74. Emans TW, Patinha D, Joles JA, Koeners MP, Janssen BJ, Krediet CTP. Angiotensin II-induced hypertension in rats is only transiently accompanied by lower renal oxygenation. *Sci Rep*. 2018;8:16342. doi: 10.1038/s41598-018-34211-2
75. Xu Z, Li W, Han J, Zou C, Huang W, Yu W, Shan X, Lum H, Li X, Liang G. Angiotensin II induces kidney inflammatory injury and fibrosis through binding to myeloid differentiation protein-2 (MD2) [published correction appears in *Sci Rep*. 2021;11:15820. doi: 10.1038/s41598-021-94987-8]. *Sci Rep*. 2017;7:44911. doi: 10.1038/srep44911
76. Nwiia SM, Leite AP, Li XC, Zhuo JL. Sex differences in the renin-angiotensin-aldosterone system and its roles in hypertension, cardiovascular, and kidney diseases. *Front Cardiovasc Med*. 2023;10:1198090. doi: 10.3389/fcvm.2023.1198090
77. White MC, Fleeman R, Arnold AC. Sex differences in the metabolic effects of the renin-angiotensin system. *Biol Sex Differ*. 2019;10:31. doi: 10.1186/s13293-019-0247-5
78. Mishra JS, Hankins GD, Kumar S. Testosterone downregulates angiotensin II type-2 receptor via androgen receptor-mediated ERK1/2 MAP kinase pathway in rat aorta. *J Renin Angiotensin Aldosterone Syst*. 2016;17:1470320316674875. doi: 10.1177/1470320316674875
79. Stoberock K, Kölbel T, Atlihan G, Debus ES, Tsilimparis N, Larena-Avellaneda A, Behrendt CA, Wipper S. Gender differences in abdominal aortic aneurysm therapy—a systematic review. *Vasa*. 2018;47:267–271. doi: 10.1024/0301-1526/a000703